Available online at www.sciencedirect.com
SCIENCE DIRECT®
International Journal of Heat and Mass Transfer 49 (2006) 1242–1254
International Journal of HEAT and MASS TRANSFER
www.elsevier.com/locate/ijhmt

Inverse method for electrodiffusional diagnostics of flows

F. Rehimi [a,b,c], F. Aloui [a,*], S. Ben Nasrallah [b], L. Doubliez [a], J. Legrand [c]

[a] Université de Nantes, Faculté des Sciences et des Techniques, Département de Physique, Laboratoire GEPEA, CNRS-UMR 6144, 2, rue de la Houssinière, BP 92208, 44322 Nantes Cedex 03, France
[b] Université du Centre, Ecole Nationale d'Ingénieurs, Laboratoire LESTE, Avenue Ibn El Jazzar 5019, Monastir, Tunisia
[c] CRTT, GEPEA, CNRS-UMR 6144, Boulevard de l'Université, BP 406, 44602 Saint-Nazaire Cedex, France

Received 13 April 2005; received in revised form 25 August 2005
Available online 6 December 2005

Abstract

The electrochemical technique is commonly used to measure the instantaneous mass transfer between a liquid consisting of an electrochemical solution and a small probe mounted flush in an inert wall. The local mass transfer allows the calculation of the instantaneous wall shear rate averaged on the probe surface. In practice, there are different models used for the calculation of the wall shear rate (Levêque solution, transfer function and Sobolik methods). The probe inertia is closely dependent on its length; a small probe allows to enlarge the band-width of the probe response. For small probes, the axial diffusion can become important in contradiction with the assumptions used in the different models. In this paper, an inverse sequential algorithm of the convection diffusion equation is applied to simulated periodic signals in order to obtain the "true" wall shear rate. A comparison between the different methods is made for different amplitudes and frequencies of wall shear rate oscillations. The influence of noise on the different methods for wall shear rate calculation is also investigated.

Keywords: Electrochemical method; Inverse method; Wall shear rate; Sequential estimation; Mass transfer

1. Introduction

The electrochemical technique is one of the non-intrusive methods used for the measurement of the local wall shear rate. It is based on the determination of the limiting diffusion current delivered by a small probe placed on an inert wall in contact with the liquid flow. By solving the convection–diffusion equation in steady regime and without the axial diffusion term, Reiss and Hanratty [1] have proposed a solution relating the limiting diffusion current and the wall shear rate. This solution is only valid for high Peclet numbers where the axial diffusion term can be neglected, and it is known as the "Levêque solution" [2].

Several authors have taken into account the axial diffusion term to obtain a solution for small Peclet numbers [3–5]. For quasi-steady regime, the Levêque solution can only be used for high Peclet numbers. For high frequency fluctuating flow, the Levêque solution cannot predict the real wall shear rate, an attenuation of the signal fluctuation and a phase shift are observed. These discrepancies are caused by the capacitive effect of the concentration boundary layer, which is acting as a low-pass filter.

In the literature, the most common approaches related to the wall shear stress probes are focused on the research of transfer functions between wall shear stress and limiting diffusion current [6–11]. In these works, the axial diffusion mass transfer was neglected and they are generally based on a linearization of the problem by assuming that the wall shear rate fluctuations remain small in comparison with the average value. When the fluctuations are important, the linear approach fails. In fact, Tu and Ramaprian [12] have met difficulties in the interpretation of their measurements obtained by hot film anemometry in the case of a flow with large oscillation amplitude. Kaiping [13] has numerically

* Corresponding author. Tel.: +33 2 51 12 55 07; fax: +33 2 51 12 55 05.
E-mail address: fethi.aloui@univ-nantes.fr (F. Aloui).

0017-9310/$ - see front matter © 2005 Elsevier Ltd. All rights reserved.
doi:10.1016/j.ijheatmasstransfer.2005.10.008

Nomenclature

A_s	active surface of the probe (m^2)
$b(t)$	Sherwood number perturbation (dimensionless)
C_0	bulk concentration (mol m^{-3})
C	concentration of active ion (dimensionless)
c	concentration of active ion (mol m^{-3})
$\tilde{c}$	complex concentration fluctuations (dimensionless)
D	diffusion coefficient (m^2 s^{-1})
F	Faraday number
f	frequency (Hz)
$H(\sigma)$	complex transfer function
$H(0)$	transfer function at very low frequencies
I	limiting diffusion current (A)
ℓ	probe width (m)
n	number of electrons exchanged in a stoichiometric reaction
Pe	Peclet number (dimensionless)
S	wall shear stress (s^{-1})
S_{des}	wall shear stress using Deslouis transfer function (s^{-1})
S^*_{lev}	$S^*_{lev} = \frac{1}{Pe}\left(\frac{Sh}{0.807}\right)^3$
S_{sob}	wall shear stress using Sobolik et al. method (s^{-1})
S_q	quasi-steady solution of the wall shear stress (s^{-1})
Sc	Schmidt number (dimensionless)
Sh	Sherwood number (dimensionless)
t	time (s)
T	period (s)
FT	Fourier transform
x, y	cartesian coordinates (m)

Greek symbols

δ_c	mass sub-layer scale (m)
β	wall shear rate fluctuation amplitude
θ	characteristic time of the probe (s)
σ	dimensionless frequency
υ	kinematic viscosity (m^2 s^{-1})

Superscripts and subscripts

–	time average
*	dimensionless form
~	complex function or parameter
^	first estimation of the data
q	quasi-steady state

studied the response of a probe to the wall shear rate consisting of a constant term with superposed sinusoidal fluctuations with large amplitude. When fluctuations become important, he noticed that the average value given by the probe departed from the Levêque solution. These results are in keeping with the recent study of Funfshilling [14] for the same type of the flow pulsation. Sobolik et al. [15] have introduced another technique based on the correction of the wall shear rate obtained by the Levêque solution by adding a term deduced from the transitory response of a probe multiplied by the time derivative of mass transfer rate. This method correctly predicts the wall shear rate for high average Peclet numbers when the sampling rate is sufficient. For low Peclet numbers, the determination of the wall shear stress needs to solve the inverse problem by using the inverse technique. The technique is often used in heat transfer problems for the determination of unknown heat flux at the boundary of an object by measuring the temperature inside it [16]. This technique, named by sequential estimation method or function specification method and introduced by Beck et al. [17], consists in solving the direct heat conduction problem and in estimating sequentially the heat flux at the boundaries by minimizing the difference between measured and simulated temperatures. For mass transfer problems, the heat conduction equation is replaced by the convection–diffusion equation, the temperature measurement by the mean concentration gradient on the probe surface and the heat flux is replaced by the unknown wall shear rate. This method was adopted for the first time by Mao and Hanratty [18,19]. In their case, they assumed that the axial diffusion is negligible. Later, Maquinghem [20] extended these works by taking into account the tangential diffusion in three-dimensional case.

In this study, the sequential estimation technique is applied to the convection–diffusion equation. The purpose is to determine the ''true'' wall shear rate from the measured limiting diffusion current, by combining the resolution of the direct convection–diffusion problem with the function specification method [21–23]. The method is tested with known solutions of the diffusion–convection equation, and then it is compared with other solutions for the determination of the wall shear rate in flows with sinusoidal fluctuations. The aim is to determine the efficiency of each method. Finally, the influence of noise on theses methods is analyzed.

2. Direct problem formulation

2.1. Introduction

An electrochemical cell consists of two electrodes (Fig. 1). The working electrode has a very small dimension to allow a local study of the mass transfer phenomena. The counter-electrode has a great dimension to have diffusion control on the working electrode only. The polarization voltage is chosen to obtain a diffusional plateau on current-voltage curves, which also corresponds to a zero

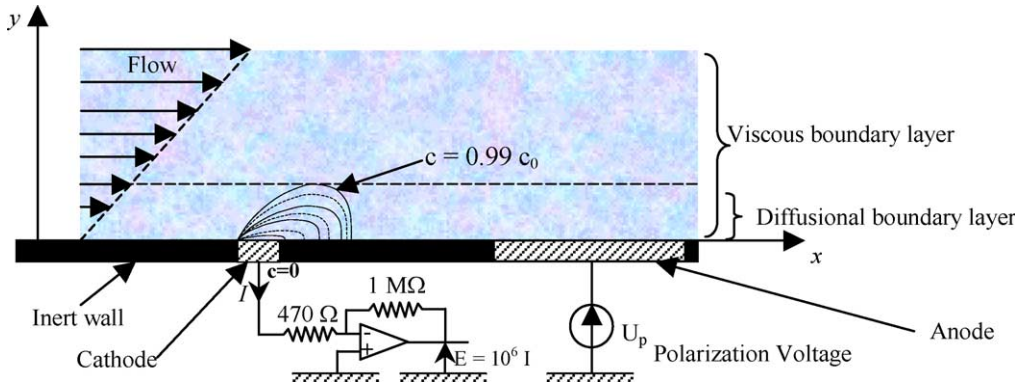

Fig. 1. Sketch of a single electrochemical cell.

concentration of reacting ion on the probe surface. In this case, the limiting diffusion current delivered by the probe can be written as:

$$I = nF \int\int_{A_s} \left(-D\frac{\partial c}{\partial y}\right)_{y=0} \mathrm{d}A = nFc_0 \frac{D}{\ell} A_s Sh \tag{1}$$

where c_0 is the initial concentration of the reactive ion, A_s the active surface of the probe, ℓ the width of the rectangular probe, D the diffusion coefficient, F the Faraday number, n the number of electrons exchanged by a stoichiometric reaction and Sh the Sherwood number. The Sherwood number is a dimensionless number proportional to the rate (mass diffusivity/molecular diffusivity (Eq. (7))).

2.2. Direct solution of the convection–diffusion problem

In the presence of an indifferent electrolyte, the general equation governing the mass transfer can be written as:

$$\frac{\partial c}{\partial t} + \vec{U} \cdot \mathrm{grad}(c) = D\Delta c \tag{2}$$

where Δ is the Laplacian of the concentration c.

In the viscous boundary layer, the axial velocity component can be written: $U_x = S(x,t)y$, where $S(x,t) = \left(\frac{\partial U_x}{\partial y}\right)_{y=0}$ is the instantaneous normal wall velocity gradient. When the probe length is small with respect to the characteristic length of the wall shear rate variations, a homogeneous wall shear rate, $S(t)$, can be assumed on the microelectrode surface. In this case, Eq. (2) becomes:

$$\frac{\partial c}{\partial t} + S(t)y\frac{\partial c}{\partial x} = D\left(\frac{\partial^2 c}{\partial x^2} + \frac{\partial^2 c}{\partial y^2}\right) \tag{3}$$

If f is a characteristic frequency of the flow, ℓ the probe width, c_0 the bulk concentration and $\overline{S}$ the time average (over several periods) of the wall shear gradient, the dimensionless form of Eq. (3) can be written as:

$$f^*\overline{Pe}^{-2/3}\frac{\partial C}{\partial t^*} + S^* y^* \frac{\partial C}{\partial x^*} = \overline{Pe}^{-2/3}\frac{\partial^2 C}{\partial x^{*2}} + \frac{\partial^2 C}{\partial y^{*2}} \tag{4}$$

with $x^* = \frac{x}{\ell}$, $y^* = \frac{y}{\delta_c}$, $t^* = tf$, $C = \frac{c}{c_0}$, $S^* = \frac{S}{\overline{S}}$, $\delta_c = \left(\frac{\ell D}{\overline{S}}\right)^{1/3}$, $f^* = \frac{f\ell^2}{D}$ a dimensionless frequency and $\overline{Pe} = \frac{\overline{S}\ell^2}{D}$ the averaged Peclet number.

The boundary conditions are presented in (Fig. 2a). The grid used is sufficient for reversing flow cases. The network grid on the probe surface is not regular in order to take into account the physical discontinuity between the wall and the probe.

A finite volume method is used for Eq. (4) discretization. An unconditionally stable implicit approach with upwind scheme has been employed [24]. The grid (Fig. 2a) used is structured and variable to allow a good accuracy.

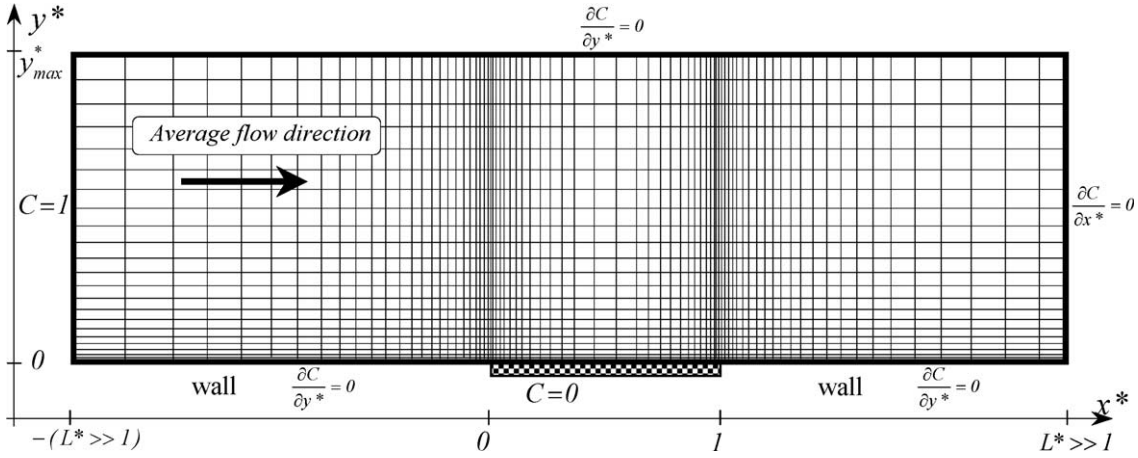

Fig. 2a. Calculation area.

In the calculation domain, if δV is the sub-volume surrounding point $P(x_i, y_j)$ (Fig. 2b), the integration of Eq. (4) over δV leads to

$$\int_t^{t+\Delta t}\int_{x_i-\frac{\delta x_{i-1}}{2}}^{x_i+\frac{\delta x_i}{2}}\int_{y_j-\frac{\delta y_{j-1}}{2}}^{y_j+\frac{\delta y_j}{2}}\left(f^*\overline{Pe}^{-2/3}\frac{\partial C}{\partial t}+S^*y\frac{\partial C}{\partial x}\right.$$
$$\left.=\overline{Pe}^{-2/3}\frac{\partial^2 C}{\partial x^2}+\frac{\partial^2 C}{\partial y^2}\right)\mathrm{d}x\,\mathrm{d}y\,\mathrm{d}t \quad (5)$$

After integration and discretization, Eq. (5) can be written as

$$a_{i,j}C_{i,j}^{t+\Delta t}=a_{i+1,j}C_{i+1,j}^{t+\Delta t}+a_{i-1,j}C_{i-1,j}^{t+\Delta t}+a_{i,j-1}C_{i,j-1}^{t+\Delta t}$$
$$+a_{i,j+1}C_{i,j+1}^{t+\Delta t}+a_{i,j}^0C_{i,j}^t \quad (6)$$

where

$$a_{i,j}^0=\frac{f^*\overline{Pe}^{-2/3}(\delta x_i+\delta x_{i-1})(\delta y_j+\delta y_{j-1})}{4\Delta t}$$

$$a_{i-1,j}=\left(\frac{\overline{Pe}^{-2/3}}{\delta x_{i-1}}+\frac{\varepsilon_s S^*}{2}\left(2y_j+\frac{\delta y_j-\delta y_{j-1}}{2}\right)\right)\left(\frac{\delta y_j+\delta y_{j-1}}{2}\right)$$

$$a_{i+1,j}=\left(\frac{\overline{Pe}^{-2/3}}{\delta x_i}+\frac{(\varepsilon_s-1)S^*}{2}\left(2y_j+\frac{\delta y_j-\delta y_{j-1}}{2}\right)\right)\left(\frac{\delta y_j+\delta y_{j-1}}{2}\right)$$

$$a_{i,j-1}=\frac{1}{\delta y_{j-1}}\left(\frac{\delta x_i+\delta x_{i-1}}{2}\right)$$

$$a_{i,j+1}=\frac{1}{\delta y_j}\left(\frac{\delta x_i+\delta x_{i-1}}{2}\right)$$

$$\varepsilon_s=\begin{cases}1 & \text{if } S^*\geqslant 0\\ 0 & \text{if } S^*<0\end{cases}$$

After this discretization, the matrix system can be written as $A\cdot\vec{C}=\vec{B}$, where

$$A=\begin{pmatrix}\cdots & 0 & 0 & \cdots\\ 0 & \ddots & \ddots & 0\\ 0 & \ddots & \ddots & 0\\ \cdots & 0 & 0 & \cdots\end{pmatrix}\Bigg\}N_xN_y \qquad \vec{C}=\begin{pmatrix}C_{1,1}^{t+\Delta t}\\ C_{1,2}^{t+\Delta t}\\ \vdots\\ C_{1,N_y}^{t+\Delta t}\\ C_{2,1}^{t+\Delta t}\\ \vdots\\ C_{i,j}^{t+\Delta t}\\ \vdots\\ C_{i,N_y}^{t+\Delta t}\\ \vdots\\ C_{Nx,Ny}^{t+\Delta t}\end{pmatrix} \qquad \vec{B}=\begin{pmatrix}a_{1,1}^0\cdot C_{1,1}^t\\ a_{1,2}^0\cdot C_{1,2}^t\\ \vdots\\ a_{1,N_y}^0\cdot C_{1,N_y}^t\\ a_{2,1}^0\cdot C_{2,1}^t\\ \vdots\\ a_{i,j}^0\cdot C_{i,j}^t\\ \vdots\\ a_{i,N_y}^0\cdot C_{i,N_y}^t\\ \vdots\\ a_{Nx,Ny}^0\cdot C_{Nx,Ny}^t\end{pmatrix}$$

N_xN_y (under A)

$[A]$ is a sparse matrix. By using the YSMP method [25], only non-null elements and their positions in the matrix are stored. The numerical resolution was made using the Bi-Conjugate Gradient method Stabilized (Bi-CG-stab),

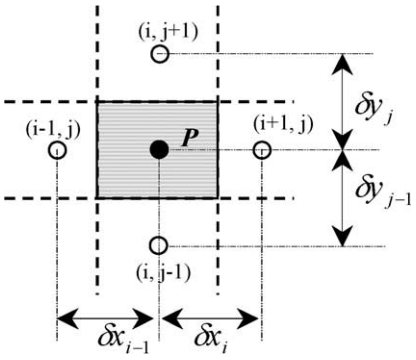

Fig. 2b. Integration sub-volume.

an SSOR preconditioning of the matrix was adopted [26]. The Sherwood number is defined by

$$Sh(t^*)=\overline{Pe}^{\frac{1}{3}}\int_0^1\left(\frac{\partial C}{\partial y^*}\right)_{y^*=0}\mathrm{d}x^* \quad (7)$$

The integration of (7) is calculated by using the Simpson method. All the calculations were done in double precision. In order to validate the numerical resolution of the diffusion convection equation, the numerical results were compared with two different analytical solutions: the Levêque solution and non stationary diffusion equation (Fick's Second Law).

In steady state regime ($S^*=1$), and by neglecting the axial diffusion term for high Peclet numbers, Eq. (4) becomes:

$$S^*y^*\frac{\partial C}{\partial x^*}=\frac{\partial^2 C}{\partial y^{*2}} \quad (8)$$

This equation has an analytic solution (the Levêque solution) [2] which can be written as

$$Sh_{\mathrm{lev}}=\overline{Sh}=0.807\overline{Pe}^{1/3} \quad (9)$$

For very high Peclet numbers, the discrepancy between our numerical solution (Eq. (4) with $f^*=0$ and $S^*=1$) and the Levêque one is less than 0.3%. The evolution of the Sherwood number with Peclet number is presented in Fig. 3a.

We notice that when the effect of the tangential diffusion becomes negligible for $\overline{Pe}$ greater than 50–100, the curve tends to the Levêque solution (9). A very important result to be noticed is that the effects of the diffusion terms can be neglected for Peclet numbers greater than $\overline{Pe} = 100$. Generally in literature, authors suggest that diffusion terms can be neglected for $\overline{Pe} \geqslant 5000$ by reference to Ling [27].

For any dimensionless wall shear gradient, the resolution of the transient diffusion equation leads to the Cottrell asymptote [28] for the first time steps with $-1/2$ slope as shown in Fig. 3b. The discrepancy between this slope and our results remains less than 0.3%.

2.3. Influence of the wall shear fluctuations on the probe response

In unsteady regime, if $Sh(t^*)$ is the measured signal, the quasi-steady shear rate is given by:

$$S_q^*(t^*) = \frac{1}{\overline{Pe}} \left(\frac{Sh(t^*)}{0.807} \right)^3 \tag{10}$$

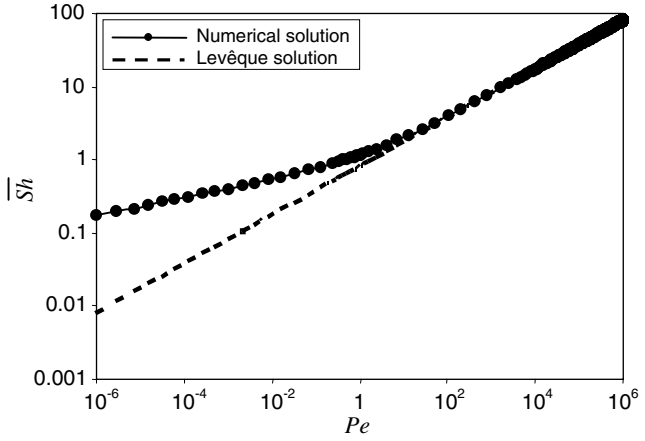

Fig. 3a. $Sh = f(Pe)$ in permanent regime.

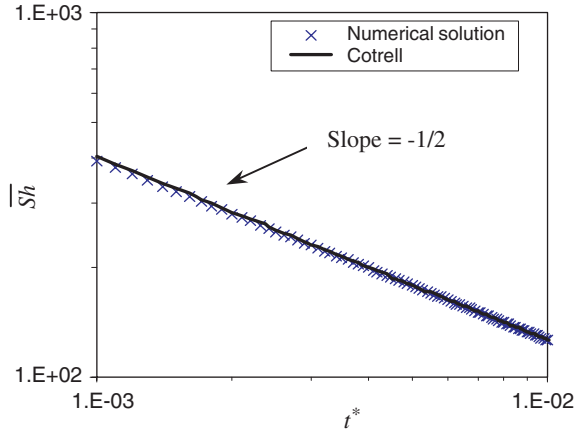

Fig. 3b. $Sh(t) = f(t)$ in transient regime.

In order to understand the behavior of an electrochemical probe in unsteady regime, a wall shear rate is considered in the following form:

$$S^*(t^*) = 1 + \beta \cos(2\pi t^* + \varphi) \tag{11}$$

In this case, $S_q^*(t^*)$ can be written as: $S_q^*(t^*) = 1 + \beta_q \cos(2\pi t^* + \varphi_q)$.

The $Sh(t^*)$ was calculated using (4) for different f^* and β values, and permitted using (10) to estimate the mean wall shear rate which was compared with the real one (Fig. 4). For an ideal probe with no inertia, the rate $\overline{|S_q^*|}/\overline{|S^*|}$ is equal to 1. For a real probe and for non-reversing flows ($\beta < 1$), the difference between the mean wall shear rate and the mean quasi-steady one can reach 5% for $f^* \leqslant 500$ and ($\beta \geqslant 0.5$) (Fig. 4).

For reversing flows ($\beta > 1$), it can be observed that the difference between $\overline{|S_q^*|}$ and $\overline{|S^*|}$ becomes very important when f^* increases. In fact, at high frequency, the concentration boundary layer is insensitive to fluctuations and the mean wall shear rate is $\overline{S^*} \approx S_{\text{lev}}^* = \frac{1}{Pe} \left(\frac{\overline{Sh}}{0.807} \right)^3$.

In the general case, heat/mass transfer probes are used to investigate the flow hydrodynamics. Fig. 5a illustrates the influence of the frequency on the estimated β_q of β using quasi-steady solution and $\Delta\varphi_q$ in Fig. 5b represents

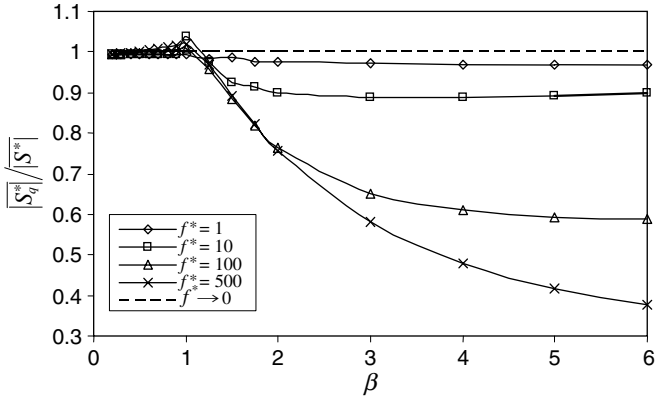

Fig. 4. Influence of the dimensionless frequency f^* and β on the mean value of the quasi-steady solution.

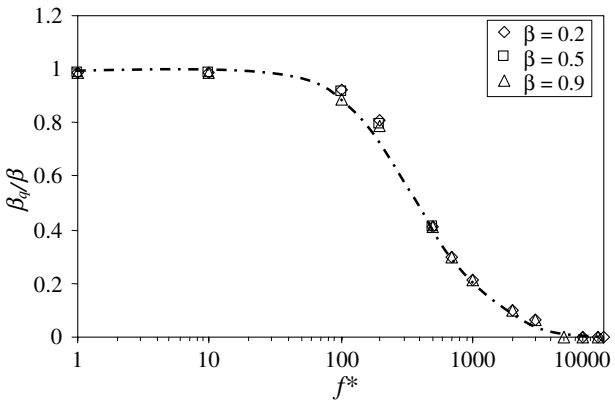

Fig. 5a. Dependence of β_q attenuation on the frequency for different β.

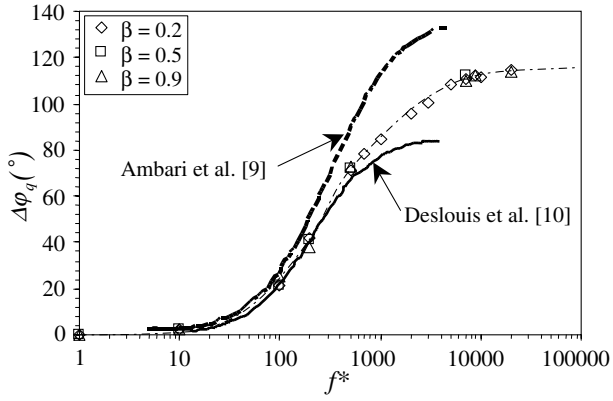

Fig. 5b. Dependence of the phase shift on the frequency for different β.

the phase shift between the quasi-steady solution and the real wall shear rate. The calculation of the fluctuation rate using quasi-steady solution is only valid for low frequencies. At high frequencies, β_q is attenuated (Fig. 5a). The vulnerability of the quasi-steady solution at high frequency is also noted in the apparition of a phase shift between the Levêque solution and the real wall shear (Fig. 5b). In fact, this departure from quasi-steady solution is due to the concentration of the sub-layer inertia. For very high frequencies ($f^* = 10^4$, for example), the phase shift is equal to $\Delta\varphi_k = \varphi - \varphi_q \approx 112°$. It is noted that $\Delta\varphi_k$ is deduced from the cross-correlation between S^* and S^*_q.

3. Formulation of the inverse problem

Inverse methods are based on the minimization of the difference between experimental results and those found by a direct model describing the phenomena (Fig. 6a) in order to determine unknown parameters or functions.

Our work is based on the use of the sequential estimation algorithm [16,17] to find the wall shear rate $S^*_{\text{exp}}(t^*)$. This approach is well adapted and usually used in heat transfer problems to determine an unknown heat flux [16,17]. The model in our case is the convection–diffusion (4).

In sequential estimation method, $S^*_{\text{exp}}(t^* \leqslant t^*_{i-1})$ is assumed to be known. Now at the time t^*_i, we define $\hat{S}^*_{\text{num}}(t^*_i)$ as the first guess of $S^*_{\text{exp}}(t^*_i)$. $\hat{S}^*_{\text{num}}(t^*_i)$ must be a good estimation of $S^*_{\text{exp}}(t^*_i)$. A Taylor series expansion truncated at first order allows to write:

$$Sh_{\text{exp}}(t^*_i) = \hat{S}h_{\text{num}}(t^*_i) + \left(S^*_{\text{exp}}(t^*_i) - \hat{S}^*_{\text{num}}(t^*_i)\right)\left(\frac{\partial \hat{S}h_{\text{num}}(t^*_i)}{\partial S^*}\right)_{\hat{S}^*_{\text{num}}(t^*_i)} \tag{12}$$

From (12), the iterative sequential process of inversion is given by:

$$S^*_{\text{exp}}(t^*_i) = \hat{S}^*_{\text{num}}(t^*_i) + \frac{\left(Sh_{\text{exp}}(t^*_i) - \hat{S}h_{\text{num}}(t^*_i)\right)}{\left(\frac{\partial \hat{S}h_{\text{num}}(t^*_i)}{\partial S^*}\right)_{\hat{S}^*_{\text{num}}(t^*_i)}} \tag{13}$$

$\frac{\partial \hat{S}h_{\text{num}}(t^*_i)}{\partial S^*}$ is estimated numerically by the following equation:

$$\left(\frac{\partial \hat{S}h_{\text{num}}(t^*_i)}{\partial S^*}\right)_{\hat{S}^*_{\text{num}}} = \frac{\hat{S}h_{\text{num}}\left(t^*_i, (1+\varepsilon)\hat{S}^*_{\text{num}}\right) - \hat{S}h_{\text{num}}\left(t^*_i, (1-\varepsilon)\hat{S}^*_{\text{num}}\right)}{2\varepsilon \hat{S}^*_{\text{num}}} \tag{14}$$

According to Beck et al. [17], ε can be chosen between 10^{-6} and 10^{-3}. In our case, the ε value used is chosen equal to 10^{-4} in order to obtain a linear evolution between $Sh(t^*_i)$and $S^*(t^*_i)$ (Fig. 6b). For values of ε less than 10^{-4}, we noted that the computation results remain unchanged.

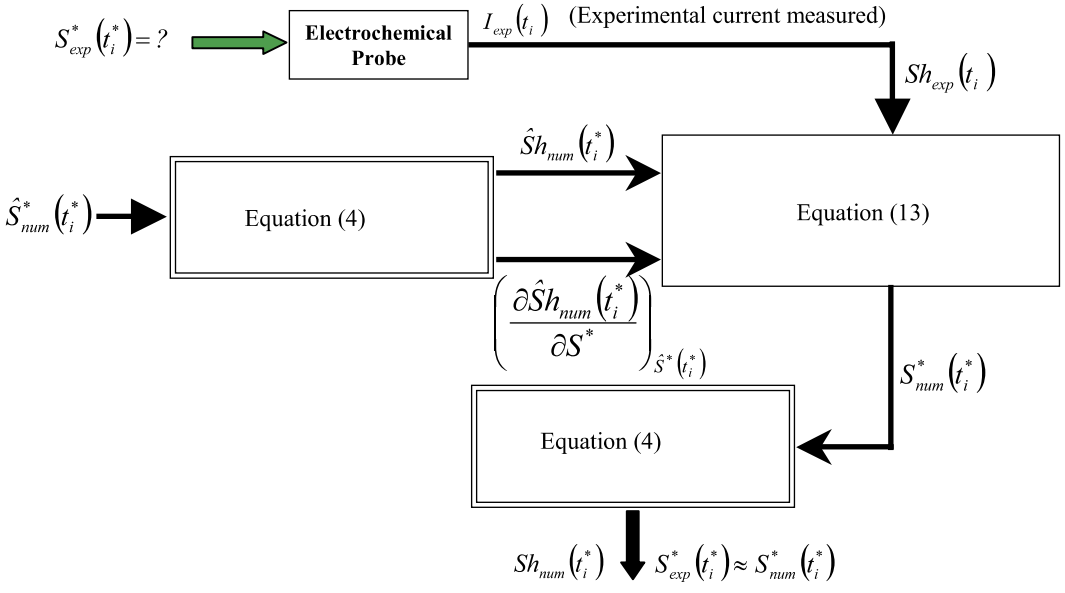

Fig. 6a. Inversion process.

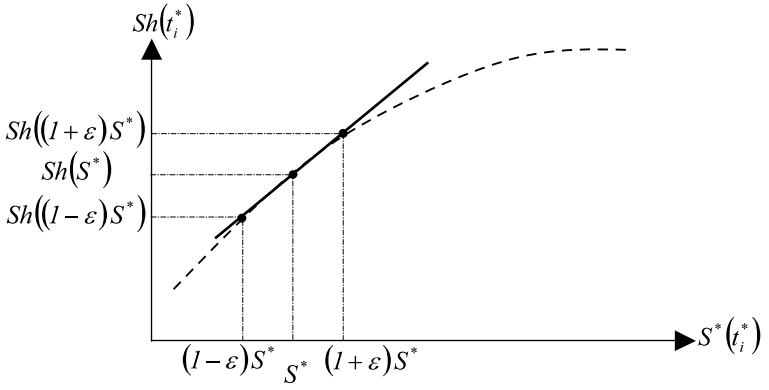

Fig. 6b. Linearization between $Sh(t_i^*)$ and $S^*(t_i^*)$.

The new value of the wall shear rate $S^*_{\text{num}}(t_i^*)$ is closer to the real wall shear rate $S^*_{\text{exp}}(t_i^*)$ to be found. This value of the wall shear rate is newly injected in the model in order to update the numerical Sherwood number at time t_i^*. After this operation, the time is incremented and the operation is repeated. The first guess $\hat{S}^*_{\text{num}}(t^* = t_0^* = 0)$ is calculated from (4) in permanent regime.

Often, for the stability of the inversion process algorithm, one assumes that the wall shear rate $\hat{S}^*_{\text{num}}(t_i^*) = \hat{S}^*_{\text{num}}(t_{i+1}^*) = \cdots = \hat{S}^*_{\text{num}}(t_{i+r}^*)$ and the computation of the wall shear rate is calculated by the following expression [16,17]:

$$S^*_{\text{num}}(t_i^*) = \hat{S}^*_{\text{num}}(t_i^*) + \frac{\sum_{k=1}^{r}\left(Sh_{\text{exp}}(t_{i+k}^*) - \hat{S}h_{\text{num}}(t_{i+k}^*)\right)\cdot\left(\frac{\partial \hat{S}h_{\text{num}}}{\partial S^*}\right)_{\hat{S}^*_{\text{num}}}}{\sum_{k=1}^{r}\left(\left(\frac{\partial \hat{S}h_{\text{num}}}{\partial S^*}\right)_{\hat{S}^*_{\text{num}}}\right)^2} \tag{15}$$

In practice, it would be better to work with the smallest value of r in order to avoid the introduction of a bias ($r = 1$ in Section 5.2).

The algorithm of estimation is presented as follows:

(i) Calculate the concentration field $C(x^*, y^*, t_i^*)$ by solving (4) with $\hat{S}^*_{\text{num}}(t_i^*) = S^*_{\text{num}}(t_{i-1}^*)$ or $\hat{S}^*(t_i) = 2S^*_{\text{num}}(t_{i-1}^*) - S^*_{\text{num}}(t_{i-2}^*)$.

(ii) Calculate $\left(\frac{\partial \hat{S}h_{\text{num}}(t_i^*)}{\partial S^*}\right)_{S^* = \hat{S}(t_i^*)}$ using (14) by solving (4) at t_i^* for the wall shear rate $(1+\varepsilon)\hat{S}^*_{\text{num}}(t_i^*)$ which allows to calculate $\hat{Sh}_{\text{num}}(t_i^*, (1+\varepsilon)\hat{S}^*_{\text{num}}(t_i))$ using (7) and repeat the same operation for $\hat{Sh}_{\text{num}}(t_i^*, (1-\varepsilon)\hat{S}^*_{\text{num}}(t_i^*))$.

(iii) Calculate $S^*_{\text{num}}(t_i^*)$ using (13) and recalculate $\hat{Sh}_{\text{num}}(t_i^*)$. A good stability of the algorithm and accuracy in the initialisation permit to have $|Sh_{\text{exp}}(t_i^*) - Sh_{\text{num}}(t_i^*)| < |Sh_{\text{exp}}(t_i^*) - \hat{Sh}_{\text{num}}(t_i^*)|$ and $|Sh_{\text{exp}}(t_i^*) - Sh_{\text{num}}(t_i^*)| < |Sh_{\text{exp}}(t_{i-1}^*) - Sh_{\text{num}}(t_{i-1}^*)|$.

(iv) Increment time and repeat the operations from i. When $|Sh_{\text{exp}}(t_k^*) - Sh_{\text{num}}(t_k^*)| \leqslant \varepsilon_{\text{precision}}$, the algorithm converge and we obtain $S^*_{\text{exp}}(t_k^*) \approx S^*_{\text{num}}(t_k^*)$ for $t^* \geqslant t_k^*$. The difference between the exact value of the wall shear rate and the solution obtained by the inverse method decreases automatically for each new time step and the algorithm converges quickly towards the desired precision.

For $t^* = t_0^*$, the concentration field $C(x^*, y^*, t_0)$ is calculated using (4) with $f^* = 0$ and $\hat{S}^*_{\text{num}}(t^* = t_0^*) = S^*_q(t^* = t_0^*)$. A bad initialisation of the $\hat{S}^*(t^* = t_0^*)$ and $C = C(x^*, y^*, t^* = t_0^*)$ tends to increase the time computing for the convergence using the direct solution, and may induce divergence in the sequential estimation because the first guess $(\hat{S}^*(t^* = t_0^*) = S^*_q(t^* = t_0^*)$ is not always a good estimator of $S^*_{\text{exp}}(t^* = t_0^*))$. A solution consists in supposing that $S^*_{\text{exp}}(t^*) = \alpha t^{*2} + \beta t^* + \gamma$ on a small time interval $t^* \in [t_0^*, t_0^* + \tau]$, and in estimating the parameters α, β and γ using the Gauss-Newton or Levenberg–Maquardt algorithm. This method systematically gives a good initialization of $S^*_{\text{exp}}(t^*)$ on $[t_0^*, t_0^* + \tau]$. With this method, we are sure that for every time step increment, $Sh_{\text{exp}}(t_i^*) \approx Sh_{\text{num}}(t_i^*)$ and $S^*_{\text{exp}}(t_i^*) \approx S^*_{\text{num}}(t_i^*)$.

4. Application of the sequential estimation on simulated data

In order to verify the validity of the sequential estimation, a known wall shear rate which has the following form, is tested:

$$S^*(t^*) = 1 + \beta\cos(2\pi t^* + \varphi)$$

The time evolution of the Sherwood number for different β values is obtained by solving the direct problem. To start the sequential estimation, we have used the steady solution of the Eq. (4) for a constant wall shear rate estimated from the Levêque solution and calculated for $t^* = 0$. The dimensionless concentration field is initiated by the steady concentration solution, obtained by solving the Lévêque problem. The results of this simulation, giving the comparison between the imposed and calculated Sherwood numbers and wall shear rates, are shown in Figs. 7–9 for different values of β. The sequential estimation applied to a single probe gives good results (Fig. 7) for

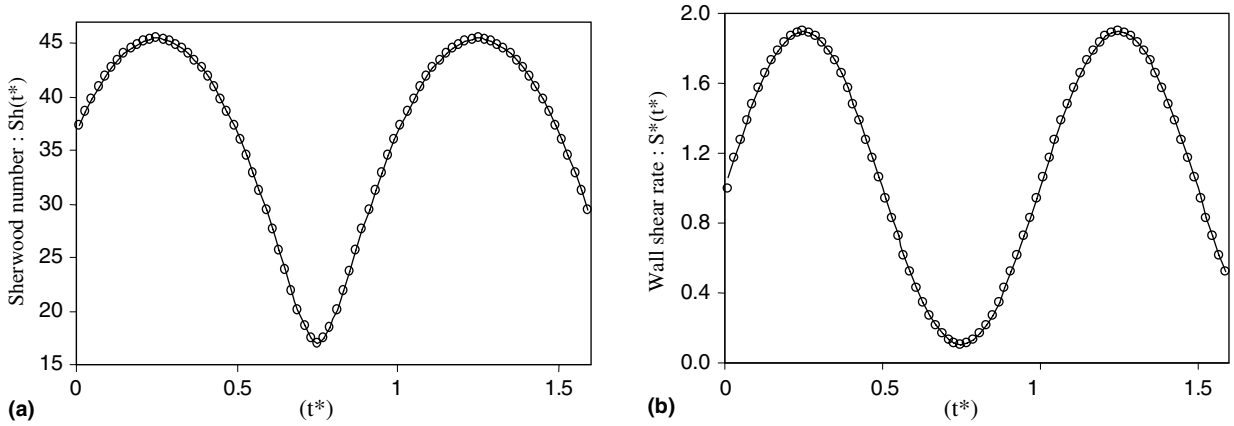

Fig. 7. Comparison between inverse method and simulated data (experimental) for $\beta = 0.9$, $f^* = 1$ and $Pe = 10^4$ (— true wall Shear rate (simulated); ○ sequential estimation): (a) Sherwood number (Sh), (b) wall shear rate (S^*).

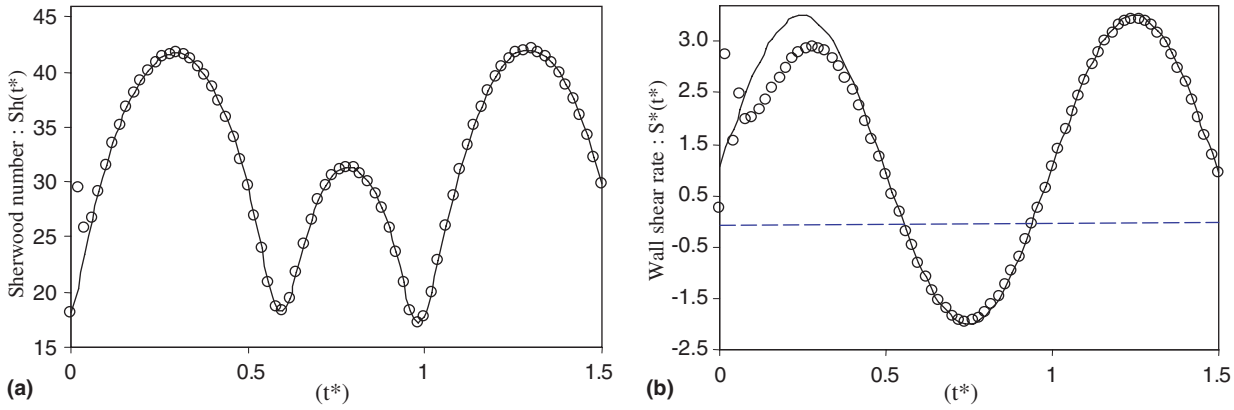

Fig. 8. Comparison between inverse method and simulated data (experimental) for $\beta = 3$, $f^* = 1$ and $Pe = 10^4$ (— true wall shear rate (simulated); ○ sequential estimation): (a) Sherwood number (Sh), (b) wall shear rate (S^*).

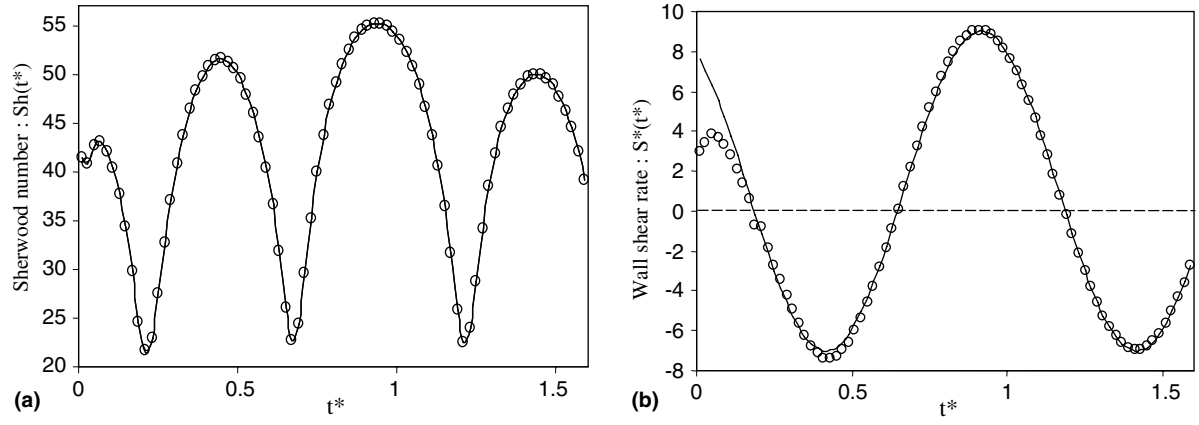

Fig. 9. Comparison between inverse method and simulated data (experimental) for $\beta = 8$, $f^* = 1$ and $Pe = 10^4$ (— true wall Shear rate (simulated); ○ sequential estimation): (a) Sherwood number (Sh), (b) wall shear rate (S^*).

the non-reversing flow cases ($\beta \leqslant 1$). If reversing flow occurs ($\beta \geqslant 1$), the inverse method gives good results but the algorithm based on Eq. (13) is numerically unstable when $\hat{S}^* \to 0$ if we take $\hat{S}^*_{\text{num}}(t^*_i) = S^*_{\text{num}}(t^*_{i-1})$. To remedy the problem, the solution consists in expressing the first guess of $\hat{S}^*_{\text{num}}(t^*_i)$ as $\hat{S}^*_{\text{num}}(t^*_i) = 2S^*_{\text{num}}(t^*_{i-1}) - S^*_{\text{num}}(t^*_{i-2})$ [21]. This expression is a consequence of derivability of the wall shear rate. The instability near $\hat{S}^* = 0$ was cited by Mao and Hanratty [18], who have assumed that it was due to the fact that they neglected the axial diffusion $\frac{\partial^2 c}{\partial x^2}$ in Eq.

(3) in their resolution. In reality, by taking into account of $\frac{\partial^2 c}{\partial x^2}$ in the resolution of the inverse problem, we stabilize the algorithm near reversing points. But in many cases, we have $S\hat{h}(t_i, \hat{S}^*_{\text{num}}) \approx S\hat{h}(t_i, -\hat{S}^*_{\text{num}})$when $\hat{S}^*_{\text{num}} \to 0$. This situation represents an ill-posed problem, especially when noised experimental signals have to be treated. According to this procedure, the simulation is also very good for reversing flows (Figs. 8 and 9: $\beta > 1$).

5. Comparison between inverse method, transfer functions and Sobolik method

In many works, the calculation of the wall shear rate from the measured limiting diffusion current is done using transfer functions between the mass transfer fluctuations and the wall shear rate fluctuations.

In this work, we have based our calculations on the transfer function proposed by Deslouis et al. [10], which is in keeping with the transfer function proposed by Nakoryakov et al. [8].

If $H(0) = \frac{1}{3}\frac{\overline{Sh}}{\overline{S}}$ and $\sigma = 2\pi f^* \overline{Pe}^{-2/3}$, for a single rectangular probe, the transfer function $H\left(=\frac{s\hat{h}}{\hat{s}}\right)$ can be written [10] as

- For $\sigma \leqslant 6$:

$$\left|\frac{H(\sigma)}{H(0)}\right| = (1 + 0.056\sigma^2 + 0.00126\sigma^4)^{-1/2} \tag{16}$$

$$\arg(H(\sigma)) = -\arctan(0.276\sigma(1 + 0.02\sigma^2 - 2.610^{-4}\sigma^4)) \tag{17}$$

- For $\sigma > 6$:

$$\left|\frac{H(\sigma)}{H(0)}\right| = \frac{1}{\sigma^{3/2}}[1 + 5.2538\sigma^{1/2} + 13.8012\sigma]^{1/2} \tag{18}$$

$$\arg(H(\sigma)) = -\arctan(1 + 1.3167\sigma^{1/2}) \tag{19}$$

The wall shear rate is calculated by writing that:

$$S_{\text{des}}(t) = \overline{S_q(t)} + \text{FT}^{-1}\left(\frac{\text{FT}(Sh(t) - \overline{Sh(t)})}{H}\right) \tag{20}$$

Sobolik et al. [15] introduced another method based on the correction of the wall shear rate calculated from the Levêque law and the transient response of the probe. They suggested that near the probe, the concentration field should be written as

$$c(x, y, t) = C_0\left(1 - G\left(\frac{y}{\delta(t)}\left(\frac{\ell}{x}\right)^{1/3}\right)\right) \tag{21}$$

where G is a decreasing function verifying $G(0) = 1$, $G(\infty) = 0$ and $G'(0) = -1$, and $\delta(t)$ is the instantaneous concentration boundary layer thickness.

By replacing the expression (21) in Eq. (4) for a negligible axial diffusion and after integration near the probe surface in the viscous boundary layer, they established that the corrected wall shear rate is:

$$S_{\text{sob}}(t) = S_q(t) + \frac{2}{3}\theta(t)\left(\frac{\partial S_q(t)}{\partial t}\right) \approx S_q(t) + 1.204\left(\frac{\partial Sh(t)}{\partial t}\right) \tag{22}$$

where

$$\theta(t) = 0.486\ell^{2/3}D^{-1/3}S_q^{-2/3} \quad \text{and} \quad S_q(t) = \frac{D}{\ell^2}\left(\frac{Sh_{\text{exp}}(t)}{0.807}\right)^3 \tag{23}$$

5.1. Influence of the frequency and the fluctuation amplitude on wall shear rate calculation for non-reversing flows

In order to test the efficiency of the different methods for different values of β and f^*, the mass transfer is simulated for a given wall shear rate by Eq. (11) for high Peclet number ($\overline{Pe} = 10^4$) in order to have a negligible axial diffusion. The comparison between the different methods will be made for $\beta \leqslant 1$ because the use of transfer function method for reversing flows is not correct and we do not know the validity of the Sobolik one for $\beta \geqslant 1$. Fourier time series decomposition was applied for $Sh(t)$ to calculate the wall shear rate using transfer function method. This decomposition is used to calculate the wall shear rate by the Deslouis et al. transfer functions and to compare the repartition of the energy on each harmonic. Tables 1–4 represent the Fourier decomposition of the wall shear rate calculated with quasi-steady solution, Deslouis transfer function, Sobolik and inverse methods.

For small dimensionless frequencies f^* ($f^* \leqslant 10$) (Fig. 10a), the quasi-steady solution is a good estimate of the wall shear rate and the correction made using transfer function or Sobolik method is not necessary. When f^* becomes important (Fig. 10b), quasi-steady solution appears to be attenuated and the phase is shifted. In fact, the quasi-steady solution gives good results for small dimensionless frequencies and high Peclet numbers because

Table 1
Repartition of the energy between harmonics for $\beta = 0.5$, f^*=1 and $Pe = 10^4$

	Fundamental	A_2	A_3	A_4	A_5	A_6	A_7	A_8	A_9
Inverse method	0.5	0	0	0	0	0	0	0	0
Quasi-steady solution	0.4999	0.0004	0.0001	0	0	0	0	0	0
Deslouis solution	0.5208	0.0461	0.0068	0.0012	0.0002	0.0001	0	0	0
Sobolik solution	0.4999	0.0002	0	0	0	0	0	0	0

Table 2
Repartition of the energy between harmonics for $\beta = 0.5$, $f^* = 500$ and $Pe = 10^4$

	Fundamental	A_2	A_3	A_4	A_5	A_6	A_7	A_8	A_9
Inverse method	0.5	0	0	0	0	0	0	0	0
Quasi-steady solution	0.2050	0.0079	0.0003	0	0	0	0	0	0
Deslouis solution	0.4750	0.0157	0.0025	0.0003	0.0001	0	0	0	0
Sobolik solution	0.4955	0.0097	0.0029	0.0003	0.0001	0	0	0	0

Table 3
Repartition of the energy between harmonics for $\beta = 1$, $f^* = 1$ and $Pe = 10^4$

	Fundamental	A_2	A_3	A_4	A_5	A_6	A_7	A_8	A_9
Inverse method	1	0	0	0	0	0	0	0	0
Quasi-steady solution	0.9833	0.0034	0.0026	0.0020	0.0017	0.0015	0.0013	0.0011	0.0010
Deslouis solution	1.4514	0.3989	0.1895	0.1094	0.0698	0.0472	0.0333	0.0243	0.0182
Sobolik solution	0.9833	0.0013	0.0007	0.0005	0.0004	0.0004	0.0004	0.0004	0.0004

Table 4
Repartition of the energy between harmonics for $\beta = 1$, $f^* = 500$ and $Pe = 10^4$

	Fundamental	A_2	A_3	A_4	A_5	A_6	A_7	A_8	A_9
Inverse method	1	0	0	0	0	0	0	0	0
Quasi-steady solution	0.4074	0.0348	0.0019	0.0004	0.0001	0	0	0	0
Deslouis solution	0.9479	0.0815	0.0234	0.0062	0.0016	0.0006	0.0001	0.0001	0
Sobolik solution	0.9842	0.0594	0.0259	0.0065	0.0017	0.0006	0.0002	0.0001	0

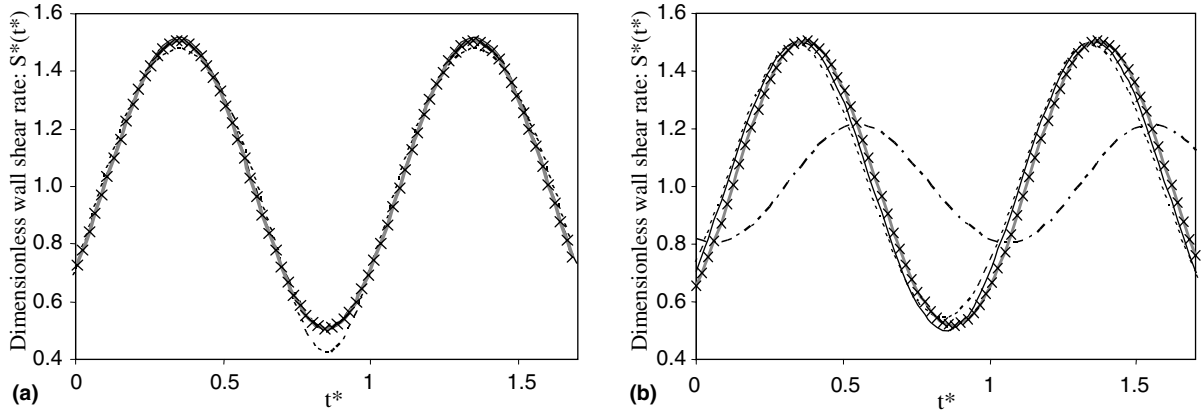

Fig. 10. Temporal comparison between wall shear rate calculated with different methods for $\beta = 0.5$ and $Pe = 10^4$ (— Inverse method; –·–·– Levêque solution; - - - Deslouis solution; ⟶ Sobolik solution): (a) $f^* = 1$; (b) $f^* = 500$.

the term $\overline{Pe}^{-2/3}\frac{\partial^2 C}{\partial x^{*2}} \ll \frac{\partial^2 C}{\partial y^{*2}}$ and the coefficient of the accumulation terms $f^*\overline{Pe}^{-2/3}\frac{\partial C}{\partial t^*}$ are very small. This situation reduces Eqs. (4)–(8), which corresponds to an ideal probe (with no inertia). In this case, the correction using transfer function and Sobolik method are very satisfactory, but the Sobolik one is more precise. By comparing the spectrum of the mass transfer evolution, we conclude that the higher order harmonics are also important and this leads to erroneous results by using the transfer functions method.

For the case corresponding to $\beta = 1$, the results are presented in Fig. 11. As we can see in Fig. 11a and in Table 3, the effect of non-linearity caused by the non-negligible energy in the higher order harmonics leads to erroneous results on the wall shear rate calculation using transfer function method. This discrepancy is attenuated for $f^* = 500$, because in such a case, the high order harmonics are automatically attenuated by the capacitive effect of the probe.

Tables 1–4 give the energy repartition between harmonics of wall shear rates for $\overline{Pe} = 10^4$. High wall shear rate fluctuations at low dimensionless frequencies, generate higher order harmonics with non negligible energy in the Sherwood number. The use of transfer function method in such a case can lead to erroneous results because the energy contained in these harmonics is amplified (Tables 1 and 3). On the contrary, this will not occur when the

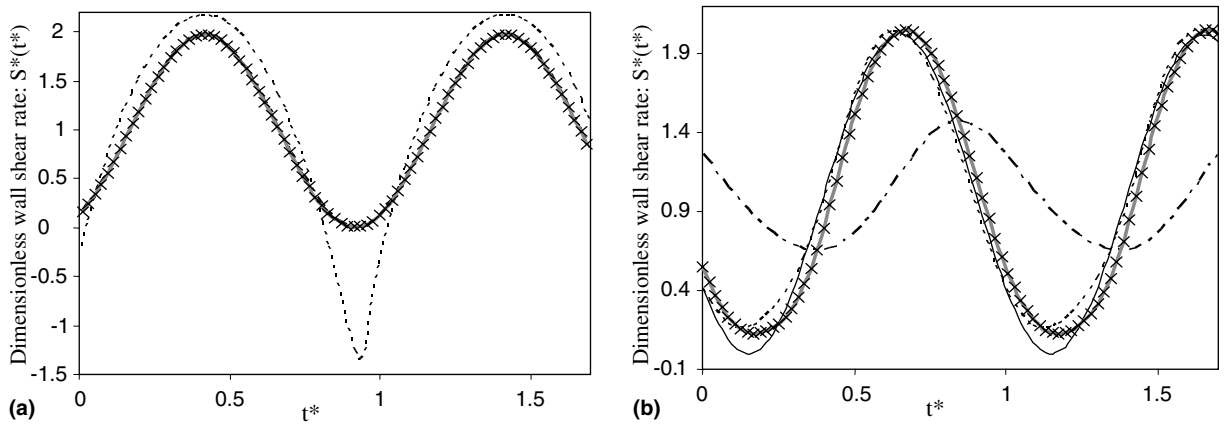

Fig. 11. Temporal comparison between wall shear rate calculated with different methods for $\beta = 1$ and $Pe = 10^4$ (— Inverse method; –·–·– Levêque solution; - - - Deslouis solution; ⟶⟵ Sobolik solution): (a) $f^* = 1$; (b) $f^* = 500$.

dimensionless frequencies are important because the higher order harmonics are attenuated by the concentration boundary layer. Moreover, the Sobolik method gives similar results like the inverse method at high Peclet numbers (axial diffusion negligible) for non-reversing flows.

5.2. Influence of the noise on wall shear rate calculation

In practice, experimental diffusion currents are often noised. So, the measured Sherwood number ${}^{m}Sh(t)$ is assumed to be the sum of the real Sherwood number ${}^{r}Sh(t)$ and an added perturbation number $b(t)$ (supposed derivable):

$$ {}^{m}Sh(t) = {}^{r}Sh(t) + b(t) \tag{24}$$

By supposing that the noise is small in comparison with ${}^{r}Sh(t)$ where ${}^{r}S_q(t)$ is given by Eq. (23), a first order expansion of ${}^{m}S_q(t)$ near ${}^{r}Sh(t)$ leads to:

$$ {}^{m}S_q(t) \approx {}^{r}S_q(t) + \frac{3^{r}S_q(t)}{{}^{r}Sh(t)} b(t) \tag{25}$$

Then, the noised shear stress calculated with Sobolik method is written as:

$$ {}^{m}S_{\mathrm{sob}}(t) \approx {}^{r}S_{\mathrm{sob}}(t) + \frac{3^{r}S_q(t)}{{}^{r}Sh(t)} b(t) + 1.2045 \frac{\mathrm{d}b(t)}{\mathrm{d}t} \tag{26}$$

and with the transfer function:

$$ \begin{aligned} {}^{m}S_{\mathrm{des}} &= {}^{r}S_{\mathrm{des}} + \frac{3^{r}Sq(t)}{{}^{r}Sh(t)} b(t) + \mathrm{FT}^{-1}\left(\frac{\mathrm{FT}(b(t))}{H}\right) \\ &\approx {}^{r}S_{\mathrm{des}} + \frac{3^{r}Sq(t)}{{}^{r}Sh(t)} b(t) + k(t)\frac{\mathrm{d}b(t)}{\mathrm{d}t} \end{aligned} \tag{27}$$

where FT and FT^{-1} are respectively the direct and inverse Fourier transforms of the signal, and $k(t)$ is a function calculated from Eq. (18) for high frequencies ($\sigma > 6$). For high frequency noise, calculations leads to $k(t) \in]6.288, 8.313[$. In quasi-steady solution, the perturbation added to the wall shear rate is minimized at high Peclet numbers due to the low values of the term $\frac{3}{{}^{r}Sh(t)}$. In addition to the noise $\frac{3^{r}S_q(t)}{{}^{r}Sh(t)} b(t)$ found in quasi-steady solution, the Sobolik method present another noise term $1.2045\frac{\mathrm{d}b(t)}{\mathrm{d}t}$ which represents the high frequencies noise amplification. The noise added to the wall shear rate obtained by the Deslouis transfer function is more important than that obtained by the Sobolik one. For high Peclet numbers, the noised wall shear rate calculated by inverse and Sobolik methods are very close for non reversing flows. This means that the inverse method noise amplification has the same order of magnitude as the Sobolik one. In the inverse method, high frequency noise leads to great perturbations on the inversion algorithm and causes the divergence of the numerical procedure. To solve this problem, the relation (15) is used instead of (13). The use of Eq. (15) is equivalent to a filtering of the signal. In practice, the noised signals have to be numerically filtered before applying the inverse method algorithm for the determination of the wall shear gradient.

In order to analyze the effect of the noise on the efficiency of the inverse method, we have considered the Sherwood number $Sh(t)$ obtained for the case $S^*(t^*) = 1 + 0.5\cos 2\pi t^* + \varphi)$ with $f^* = 500$ and $\overline{Pe} = 10^4$. A Gaussian noise of the form $b(t)$ where $\overline{b(t)} = 0$ and a variance equal to $10^{-2}\overline{Sh}$ is superimposed on $Sh(t)$. Therefore, the measured Sherwood number is $Sh_{\mathrm{exp}}(t) = Sh(t) + b(t)$. The results obtained by sequential estimation on Sh_{exp} with $r = 10$ are given in Figs. 12a and 12b.

The noise is dramatically amplified with the Deslouis and the Sobolik solutions. Table 5 shows the standard deviation of wall shear rate relative to each method. As mentioned before, the Deslouis solution is more vulnerable to the noise and we can observe that the latter is more amplified. The standard deviation of the Sobolik solution is twice less amplified than the Deslouis one. But this amplification remains very important compared with the inverse method. The small standard deviation value found with the inverse method is due to the filtering of the data by using $r = 10$. By varying r in the inverse method ($r > 10$ in this case), it is possible to find a value for which the noise contained in the measured signal vanishes completely.

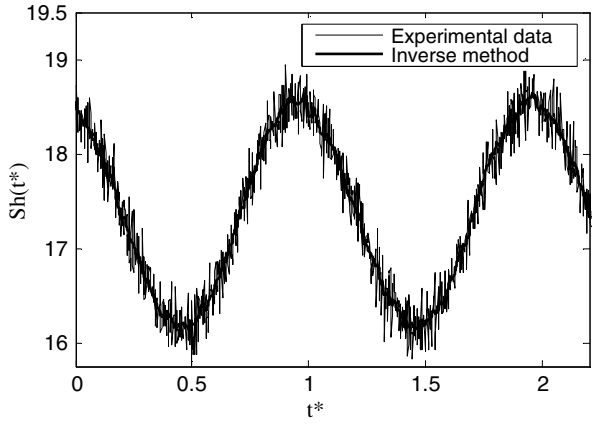

Fig. 12a. Comparison between the Sherwood number found by inverse method and the real one.

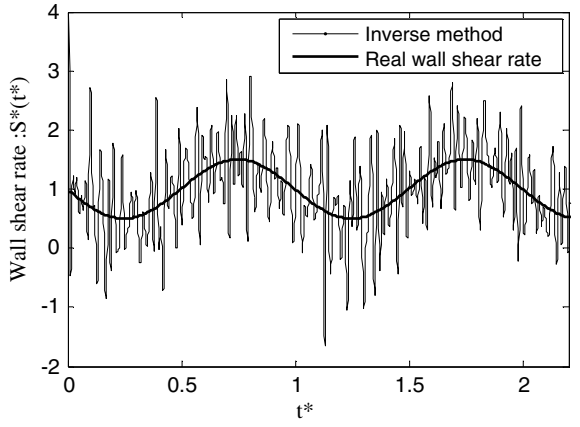

Fig. 12b. Comparison between the non noised wall shear rate and noised one found by inverse method.

Table 5
Standard deviation of the noised wall shear rate signal obtained for each method: $\beta = 0.5$, $f^* = 500$ and $\overline{Pe} = 10^4$

	Inverse solution	Quasi-steady solution	Sobolik solution	Deslouis solution
$\sqrt{\overline{(S^*(t^*)_{\text{calculated}} - S^*(t^*))^2}}$	0.93	0.34	7.47	15.34

6. Conclusion

An inverse method is established to calculate the wall shear rate from the mass transfer measured by a single electrochemical probe. The diffusion–convection equation is solved by using the finite volume method with an implicit scheme. The direct solution consists in calculating the limiting diffusion current from a known wall shear rate. The inverse technique allows to obtain the wall shear rate by minimizing the difference between the limiting diffusion current calculated by the direct solution and the measured one. Thereafter, a comparison was made between inverse technique, transfer function method and the Sobolik method. The success of the inversion process is closely linked to the sampling rate and the right initialization of both wall shear rate and concentration field. For non-reversing flows, the inverse and Sobolik methods nearly give the same instantaneous wall shear rate for high average Peclet numbers. On the contrary, the transfer function approach is not reliable for high wall shear rate fluctuations at low dimensionless frequency. The effect of noise is more visible on transfer function method. The Sobolik method and inverse technique are less sensitive to the noise, but they are affected by the high frequency noise which is amplified. Finally, in spite of its complexity, the sequential estimation (inverse method) remains the most rigorous method to be used to calculate the ''true'' wall shear rate. This method could also be judicious for solution of 3D mass transfer equation with a variable wall shear rate along the probe.

References

[1] L.P. Reiss, T.J. Hanratty, An experimental study of the unsteady nature of the viscous sub-layer, AIChE J. 9 (1963) 154–160.
[2] M.A. Levêque, Les lois de transmission de la chaleur par convection, Ann. Mines 13 (1928) 381–412.
[3] R.C. Ackerberg, R.D. Patel, S.K. Gupta, The heat/mass transfer to a finite strip at small Peclet numbers, J. Fluid Mech. 86 (1978) 49–65.
[4] P.I. Geshev, The green function method for calculating characteristics of small strip-shaped shear stress probe, J. Electroanal. Chem. 410 (1995) 1–8.
[5] H.G. Dimopoulos, T.J. Hanratty, Velocity gradient at the wall for flow around a cylinder for Reynolds numbers between 60 and 360, J. Fluid Mech. 33 (1968) 303–319.
[6] M. Lebouché, Relation entre les fluctuations pariétales du transfert massique et du gradient de vitesse dans le cas d'un nombre de Schmidt grand, Comptes Rendus de l'Académique des Sciences 271 (1970) 438–441.
[7] G. Fortuna, T.J. Hanratty, Frequency response of the boundary layer on wall transfer probes, Int. J. Heat Mass Transfer 14 (1971) 1449–1507.
[8] V.E. Nakoryakov, A.P. Budukov, O.N. Kashinsky, P.I. Geshev, Electrodiffusion method of investigation into local structures of turbulent flows, in: V.G. Gasenko (Ed.), Novosibirsk, 1986.
[9] A. Ambari, C. Deslouis, B. Tribollet, Frequency response of mass transfer rate in a modulated flow at electrochemical probes, Int. J. Heat Mass Transfer 29 (1985) 35–45.
[10] C. Deslouis, O. Gil, B. Tribollet, Frequency response of electrochemical sensors to hydrodynamics fluctuations, J. Fluid Mech. 215 (1989) 85–100.
[11] C. Deslouis, F. Huet, O. Gil, B. Tribollet, Spectral analysis of wall turbulence with a bicircular electrochemical probe, Exp. Fluids 16 (1993) 97–104.
[12] S.W. Tu, B. Ramaprian, R. Fully, Developed periodic turbulent pipe flow, Part 1: Main experimental results and comparison with predictions, J. Fluid Mech. 137 (1983) 41–58.
[13] P. Kaiping, Unsteady forced convective heat transfer from a hot film in non-reversing and reversing flow, Int. J. Heat Mass Transfer 26 (1983) 545–557.
[14] P. Funfshilling, Investigation par un écoulement de Couette de la réponse fréquentielle des sondes électrochimiques et de la floculation de particules en suspension, Ph.D. Thesis, INPL, Nancy, France, 2001.
[15] V. Sobolik, O. Wein, J. Cermak, Simultaneous measurement of film thickness and wall shear stress in wavy flow of non-Newtonian liquids, Collection Czechoslovak Chem. Commun. 52 (1987) 913–928.

[16] S. Chantasiriwan, Comparison of three sequential function specification algorithms for the inverse heat conduction problem, Int. Commun. Heat Mass Transfer 26 (1999) 115–124.
[17] J.V. Beck, B. Blackwell, C.R. St-Clair, Inverse Heat Conduction, Wiley, New York, 1985.
[18] Z. Mao, T.J. Hanratty, Analysis of wall shear stress probes in large amplitude unsteady flows, Int. J. Heat Mass Transfer 34 (1991) 281–290.
[19] Z. Mao, T.J. Hanratty, Measurement of wall shear rate in large amplitude unsteady flows, Exp. Fluids 12 (1992) 342–350.
[20] T. Maquinghen, Métrologie tridimensionnelle instationnaire à l'aide de la méthode polarographique, Ph.D. Thesis, Université de Valenciennes et du Hainaut-Cambrésis, France, 1999.
[21] D.A. Tortorelli, P. Michaleris, Design Sensitivity Analysis: Overview and review, Inverse Problems Engng. 1 (1994) 71–105.
[22] S. Chantasiriwan, An algorithm for solving multidimensional inverse heat conduction problem, Int. J. Heat Mass Transfer 44 (2001) 3823–3832.
[23] A. Bendada, M. Lamontagne, Analysis of thermal contact resistance between polymer and mold in injection molding, Appl. Therm. Engng. 24 (2004) 2029–2040.
[24] S.V. Patankar, Numerical Heat transfer fluid flow, Hemisphere/ Mc Graw-Hill, New York, 1980.
[25] G.S. Jeremy, A modern frame work for high performance linear algebra, Master Thesis, University of Notre Dame, Department of Computer Science and Engineering, Indiana, 1999.
[26] A. Markovic, an investigation of sparse matrix solvers with applications to models of transport in porous media, Master in sciences, Center in Statistical Science and Industrial Mathematics, Queensland University of Technology, 1995.
[27] S.C. Ling, Heat transfer from a small spanwise on an insulated boundary, J. Heat Transfer, Trans. ASME (1963) 230–236.
[28] V. Sobolik, J. Tihon, O. Wein, K. Wichterle, Calibration of electrodiffusion friction probes using a voltage-step transient, J. Appl. Electrochem. 28 (1998) 329–335.